RSC Advances

ROYAL SOCIETY OF CHEMISTRY

www.rsc.org/advances

Ag doped $Bi_2O_{2.33}$ Microrods: Photocatalytic Activity Investigation

Xiaojuan Wang,[a] Alei Zhu,[a] Zhiyi Li [a] and Zhijun Liu[a*]

[a] R&D Institute of Fluid and Powder Engineering, Dalian University of Technology, Dalian 116024, China

Ag doped $Bi_2O_{2.33}$ were successfully synthesized via a facile and chemical strategy, and the photocatalytic activity of the products was investigated. The crystal structure and morphology of the products were characterized by XRD, FT-IR, FESEM and HRTEM. The products show good crystallinity of body-centered tetragonal phase of $Bi_2O_{2.33}$. Results of UV-vis DRS show that Ag doped $Bi_2O_{2.33}$ exhibits stronger and broader spectral absorption than bare $Bi_2O_{2.33}$. The Ag-6% $Bi_2O_{2.33}$ was found to exhibit the highest photocatalytic activity in the Rhodamine B degradation experiments, and achieved a degradation efficiency of 93.54%; while bare $Bi_2O_{2.33}$, Ag-3%, and Ag-9% achieved degradation efficiencies of 61.93%, 73.62%, and 82.32%, respectively. The stability and reusability of Ag doped $Bi_2O_{2.33}$ was also tested. The results showed that Ag-6% $Bi_2O_{2.33}$ could obtain good degradation efficiency in five cycles reusing, 93.54%, 92.50%, 92.25%, 92.20% and 92.20%, respectively. The active species of $O_2^{\cdot-}$ and ·OH during the photodegradation process were detected by EPR technology. Ag-doped $Bi_2O_{2.33}$ is a promising photocatalyst with high photocatalytic activity and stability, showing a great potential in the field of environmental remediation.

Keywords: Ag doped $Bi_2O_{2.33}$, microrods, simulated sunlight, photocatalytic activity, Rhodamine B

1. Introduction

Bismuth oxide as multi-functional semiconductor materials has wide applications in photocatalysis,[1-4] electrochemical electrode materials,[5] optical coatings,[6] and metal/insulator/semiconductor (MIS) capacitors.[7] Bismuth oxide primarily displays four crystalline phases: monoclinic α-Bi_2O_3, tetragonal β-Bi_2O_3, body-centered cubic γ-Bi_2O_3, and face-centered cubic δ-Bi_2O_3.[8-10] Bi_2O_3 and its modifications have been investigated extensively as they are promising photocatalysts with relatively narrow band gap and higher oxidation power of the valence holes properties.[11] Also, Bi_2O_3 is used as catalysts for degradation of various organic pollutants.[12-16]

Recently, more interests are focused on the nonstoichiometric phase $Bi_2O_{2.33}$ that usually exists as impurity in the bismuth oxide thin films, bismuth oxides, and bismuth-oxide-based materials.[17-19] $Bi_2O_{2.33}$ nanosheets were synthesized by electrolytic corrosion of metal Bi, and detected one strong UV emission at room temperature; the results indicated that $Bi_2O_{2.33}$ nanosheets had a great potential to be used for UV light emitters.[20] Huang et al. prepared 3D orange-like $Bi_2O_{2.33}$ microspheres by the conventional chemical precipitation technique, and the products display super capacitive performance, suggesting the potential application in energy storage.[21] $Bi_2O_{2.33}$ nanoflowers synthesized by Guan et al. via a one-step solvothermal method, and the products display ferromagnetic signal at room temperature.[22] Although the studies of $Bi_2O_{2.33}$ some properties, such as photoluminescence, capacity and magnetism, have been conducted, to the best of our knowledge, there is no report of the photocatalytic capability of nonstoichiometric phase $Bi_2O_{2.33}$ and its modifications.

Here in, Ag doped $Bi_2O_{2.33}$ microrods are prepared by a facile method, and the optical property and photocatalytic performance of the products are also investigated. Our results show that Ag doped $Bi_2O_{2.33}$ demonstrate significantly enhanced photocatalytic activity, and has a promising application in the degradation of organic pollutants.

2 Experimental

2.1 Materials and methods

Bismuth nitrate pentahydrate ($Bi(NO_3)_3{\cdot}5H_2O$) and Rhodamine B (RhB) were purchased from Sinopharm Chemical Reagent Co., Ltd. Silver nitrate ($AgNO_3$) and sodium hydroxide (NaOH) were purchased from Tianjin Kermel Chemical Reagent Co., Ltd. Nitric acid (HNO_3) and sodium dodecyl benzene sulfonate (SDBS) were purchased from Tianjin Damao Chemical Reagent Co., Ltd. All chemical reagents were of analytical grade and used without further purification.

Ag doped $Bi_2O_{2.33}$ as photocatalyst was prepared by the co-precipitation method using $Bi(NO_3)_3{\cdot}5H_2O$ and $AgNO_3$ as starting materials. In a typical synthesis procedure: 6 mmol $Bi(NO_3)_3{\cdot}5H_2O$ and 0.18 mmol $AgNO_3$ powder were completely dissolved in 20 mL 2 mol·L^{-1} nitric acid under vigorous stirring at room temperature to obtain transparent Bi^{3+} and Ag^+ aqueous solution, with 0.05g SDBS as surfactant. 4 mol·L^{-1} NaOH was added dropwise into the above solution with the help of agitation until pH reaches to 12. After stirring for 3 h at 40 °C, the resulting mixture was then left still 4 h at room temperature. Then the slurry was centrifuged and washed

* Corresponding author: E-mail: liuzj@dlut.edu.cn, Tel.&Fax: ++86-411-84986285

several times with distilled water and absolute ethanol, and the solids were oven-dried at 60 °C for 12 h. Finally, the products were calcined at 500 °C for 4 h in air. Samples synthesized with Bi^{3+}: Ag^{+} at mole ratio of 1:0.03, 1:0.06, 1:0.09 were denoted as Ag-3%, Ag-6% and Ag-9%, respectively. For comparison, bare $Bi_2O_{2.33}$ was synthesized under same conditions without adding Ag source.

2.2 Catalyst characterization

The crystalline structures and compositions of as-prepared samples were determined by a Shimadzu XD-3A X-ray diffractometer with Cu *K*α irradiation at 30 kV and 30 mA. The surface morphology and microstructures of the samples were characterized by field-emission scanning electron microscopy (FE-SEM, Nova Nano SEM 450) and field emission (high-resolution) transmission electron microscopy (HRTEM, TF30), respectively. Fourier transform infrared spectrometer (FT-IR, EQUINOX55) spectra were recorded in the range of 400-4000 cm^{-1}. UV–vis diffuse-reflectance spectra (JASCO, UV-550) were collected in the wavelength range of 200–800 nm. Electron paramagnanetic resonance spectra (Bruker, EPR-300E) were recorded at room temperature in dark or under simulated sunlight irradiation using 5,5-dimethyl-1-pyrroline N-oxide (DMPO) as the radical trap to detect the active species during the photodegradation process.

2.3 Photocatalytic Measurement

The photocatalytic activity of the products was tested by the degradation of RhB. It was performed in a quartz reactor with a 500 W Xe lamp as the light source to simulated sunlight irradiation with wavelength range of 200–800 nm. In each experiment, 0.05 g of the as-prepared photocatalysts was added to a 50 mL RhB solution with a concentration of 20 $mg{\cdot}L^{-1}$. Before irradiation, the suspensions were magnetically stirred for 60 min in the dark to ensure the system to reach absorption-desorption equilibrium. All photocatalytic experiments were accompanied with magnetic stirring and performed under the same simulated sunlight irradiation. Upon illumination for every 30 min, 3 mL of the suspension was extracted and centrifuged (9000 rpm) for 10 min, analyzed by recording UV-vis spectra on a UV 1100 spectrophotometer. The concentration of RhB was determined at its characteristic absorption wavelength of 554 nm. Photodegradation efficiency can be calculated by the following formula:

$$\text{Photodegradation rate (\%)} = \frac{C_0 - C}{C_0} \times 100 \qquad (1)$$

where C_0 is the concentration of RhB before irradiation (t=0) and C is the concentration of RhB after a certain irradiation time.

3. Results and discussion

3.1 Crystal structure analysis

The typical XRD patterns of $Bi_2O_{2.33}$ prepared with different content of Ag are shown in Fig. 1a, suggesting the nonstoichiometric phase of $Bi_2O_{2.33}$. The characteristic peaks at 2θ of 10.06°, 20.18°, 26.38°, 29.20°, 30.42°, 32.90°, 35.68°, 45.44° and 47.22° correspond to the (004), (008), (105), (107), (00 12), (110), (00 14), (1 1 12), (200) crystalline planes of the body-centered tetragonal phase of $Bi_2O_{2.33}$ (JCPDS No.27-0051), respectively. And no impurities or other phases were observed in the as the synthesized samples. After doping with Ag, the intensity and the shape of diffraction peaks of samples have no obvious changes. A little different shift trend of (107) diffraction peak was detected in the XRD patterns for Ag-doped samples, as shown in Fig. 1b. (107) peak showed a shift to lower angle with the increase in Ag doping content. The main reason is that the doped ion radius of Ag^{+} (0.126 nm) is bigger than that of Bi^{3+} (0.096 nm). Besides, a typical pattern of the FCC (face-center cubic) structure of metallic Ag (JCPDS No.04-0783) was observed in the XRD patterns of Ag doped samples as shown in Fig. 1(d). The presence of separate Ag_2O phases was not observed due to the low dopant concentration or the substitution of Bi^{3+} lattice sites by the doped Ag^{+}. The sharp peaks indicate a good crystallinity of $Bi_2O_{2.33}$.

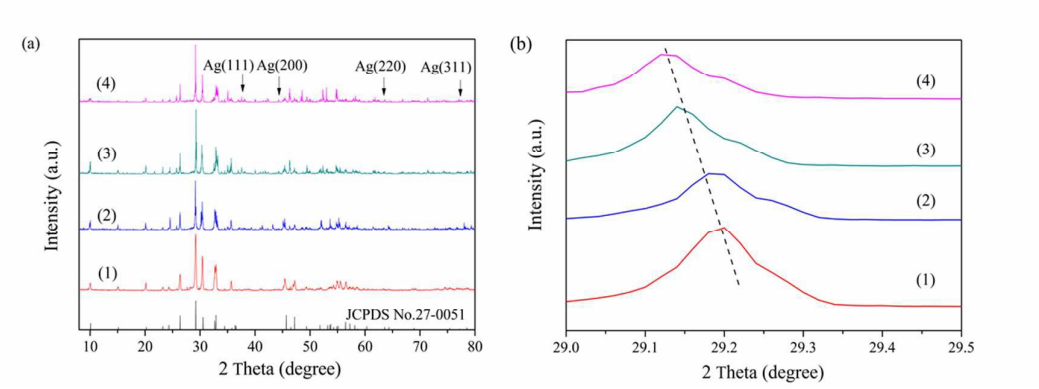

Fig. 1 XRD patterns of samples: (1) bare sample, (2) Ag-3%, (3) Ag-6%, (4) Ag-9%

The typical FTIR spectra of bare $Bi_2O_{2.33}$ and Ag-6% measured in the range of 400-4000 cm^{-1} are shown in Fig. 2. According to the study of Fruth et al. [23,24], each absorption band in the range of 200-800 cm^{-1} was attributed to the stretching vibration mode of Bi-O, taking into account the mean wavenumber and the intensity of the bands. Such phenomenon was also reported by Carrazan et al.,[25] showing that in the 400~600 cm^{-1} range, the stretching and deformation modes involving Bi-O could be observed. The absorption bands at 541 cm^{-1}, 503 cm^{-1} and 430 cm^{-1} confirm the existence of Bi-O. In addition, the appearance of sharp bands centered at ~3440 cm^{-1} and 1400 cm^{-1} indicated the existence of O-H stretching of the absorbed H_2O molecules and the carbonate moieties which are generally observed when FTIR samples were measured in air.[26,27] It was found that the FTIR spectra of Ag-6% sample, were quite similar to the bare $Bi_2O_{2.33}$ (Fig. 2), suggesting that the addition of Ag has little effect on the FTIR adsorption bands.

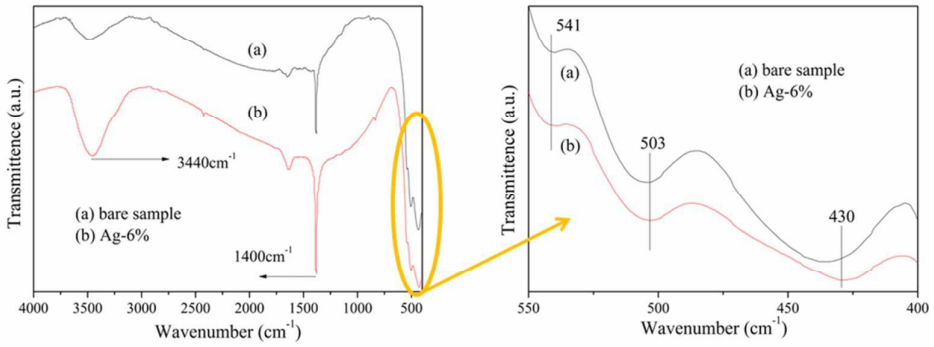

Fig. 2. FT-IR spectra of bare sample and Ag-6% doped sample

3.2 Morphological analysis

Figure 3 shows the local SEM and TEM images of $Bi_2O_{2.33}$. As presented in Fig. 3a, the Ag-6% sample appeared as microrods with a length of 4 μm and an aspect ratio of 10. Sample of Ag-6% displayed a rod shape decorated with a few nanoparticles (Fig. 3b). The prepared $Bi_2O_{2.33}$ was body-centered tetragonal phase (with lattice parameters of a=3.85 Å, b=3.85 Å, c=35.10 Å, α=90°, β=90° and γ=90°). The lattice fringe image shown in Fig. 3d clearly revealed high crystallinity of $Bi_2O_{2.33}$ rods. An HRTEM image taken from the edge in Fig. 3c showed the interplanar distances of 0.278 nm, a typical (110) plane of $Bi_2O_{2.33}$. In addition, the SAED pattern in Fig. 3c inset exhibited a body-centered tetragonal symmetric diffraction pattern that could be ascribed to single-crystalline nature of $Bi_2O_{2.33}$. However, due to the low content and well dispersion of Ag over $Bi_2O_{2.33}$ rods, no significant fringe lattices associated with Ag were detected in the HRTEM image.

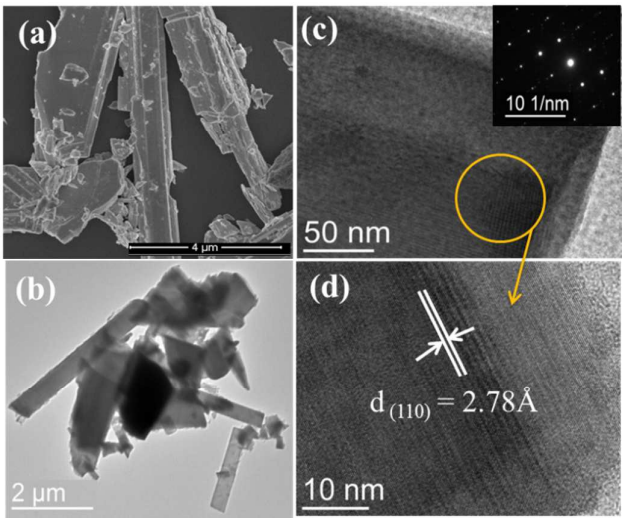

Fig. 3 SEM images of Ag-6% (a), TEM photos of Ag-6% (b-d)

3.3 Optical absorption property

The optical properties of synthesized $Bi_2O_{2.33}$ photocatalysts were studied by UV-vis DRS spectroscopy. As shown in Fig. 4a, prepared samples demonstrate good absorption performance of ultraviolet and visible light. There is a strong absorption at approximately 456 nm for all samples, which is assigned to the intrinsic band-gap absorption of $Bi_2O_{2.33}$. After Ag doped, doping samples show an additional remarkable strong and broad absorption bands in the range of 500~700 nm in visible light region. Samples doped with Ag-3%, Ag-6% and Ag-9% exhibit absorption bands centered at ~562 nm, ~574 nm and ~598 nm, respectively. There are similar results found in precious work, and the explanation might be that: the additional broad prominent absorption observed for doping samples should be attributed to the surface plasmon resonance effect of Ag; and the surface plasmon absorption on the surface of Ag derives from a collective oscillation of free electrons excited by the matching photon energy.[28–32] The absorption bands of Ag doped samples extend significantly toward visible light and the absorption intensity also increases. The doping of Ag leads to the red shift that seems more apparent in the sample with a higher Ag ratio. Therefore, the prepared samples have greater absorption efficiency at the visible light region and improved utilization of sunlight.

The band-gap energy, which represents the energy change of an electron transition from oxygen valence band (VB) to bismuth conduction band (CB), is of great significance in photocatalytic activity.[33] The band-gap energy of synthesized photocatalysts can be estimated from Tauc's plots by the following formula: [34]

$$\alpha h\nu = A(h\nu - E_g)^{n/2} \quad (2)$$

where α is the absorption coefficient near the absorption edge, $h\nu$ is the photon energy, A is a constant, E_g is the absorption band-gap energy, and n has different values depending on the absorption process. Here n=1 for the direct transition semiconductor material of bismuth oxide.[35,36] The plots of $(\alpha h\nu)^2$ versus $h\nu$ of the samples are shown in Fig. 4b. E_g is estimated by the straight portion of the $(\alpha h\nu)^2$ versus $h\nu$ plot to α = 0. Then, the band-gap energy of bare sample, Ag-3%, Ag-6% and Ag-9% is 2.70, 2.26, 2.20 and 2.14 eV, respectively.

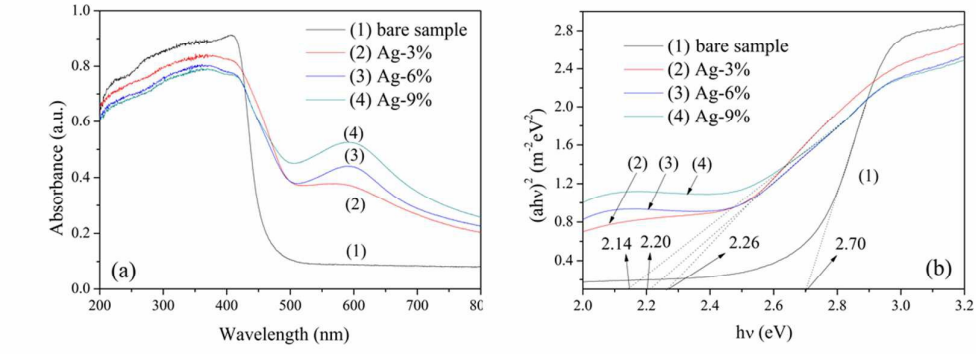

Fig. 4 (a) UV–vis DRS of synthesized samples, (b) Tauc's plots to estimate the band-gap energy (E_g).

3.4 Photocatalytic activity

The photocatalytic activity of the synthesized photocatalysts was evaluated by the photodegradation of RhB under simulated sunlight irradiation and compared with the direct photolysis (Blank). Figure 5a displays UV-vis absorbance spectra of RhB solution at different time intervals in the presence of bare $Bi_2O_{2.33}$ under simulated sunlight irradiation. Clearly, the absorption peaks at 554 nm gradually decreased with increasing irradiation time. The absorption intensity of RhB at 554 nm steadily decreased upon increasing irradiation times, in accordance with the gradual color change of the reaction solution from rich-red color to pale pink at different times (Fig. 5a, inset). Figure 5b displays the change in concentration of RhB upon irradiation time in the absence and presence of undoped and Ag-doped $Bi_2O_{2.33}$. For all the adsorption processed in dark, little difference was found on the degradation of RhB. Under the same reaction condition for 180 min, only 9.87% degradation occurred relative to the direct photolysis (Blank), whereas bare $Bi_2O_{2.33}$, Ag-3%, Ag-6% and Ag-9% achieved degradation efficiencies of 61.93%, 73.62%, 93.54% and 82.32%, respectively (Table 1). Under simulated sunlight and in the same illumination time, Ag-doped samples exhibited enhanced photocatalytic activity because of their lower band-gap energy and higher optical absorption in wider visible light region.[37]

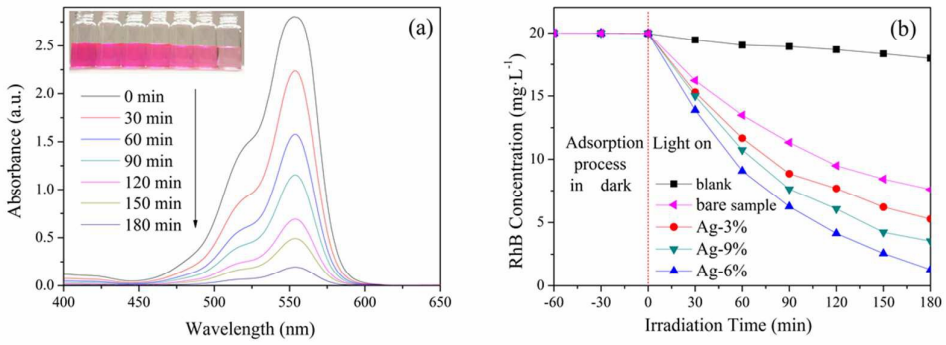

Fig. 5 (a) UV–vis spectra of an RhB solution by 6% Ag doped $Bi_2O_{2.33}$ under simulated sunlight irradiation (I_0 = 140 mW cm^{-2}). The inset shows photographs of the color change of the RhB solution during different reaction times. (b) RhB concentration varying with time over different samples.

The photodegradation of RhB by direct photolysis or photocatalysts was examined by fitting the experimental data to the following pseudo-first-order decay kinetics equation. Based on the Langmuir-Hinshelwood model,[38] the reaction rate constant can be estimated as:

$$k = -\frac{1}{t}\ln\left(\frac{C}{C_0}\right) \quad (3)$$

where C_0 and C are the initial concentration of RhB (C_0 = 20 mg·L^{-1}) and the RhB concentration at time t, and k is the first-order kinetic constant. Figure 6 shows the five fitted lines according to our photocatalysis experiments. The kinetic constants and regression coefficients (R^2) were also listed in Table 1. It was found that Ag-6% sample exhibits a photocatalytic activity of 26.5, 2.7, 2.0 and 1.5 times higher than that of direct photolysis, bare sample, Ag-3% and Ag-9%, respectively.

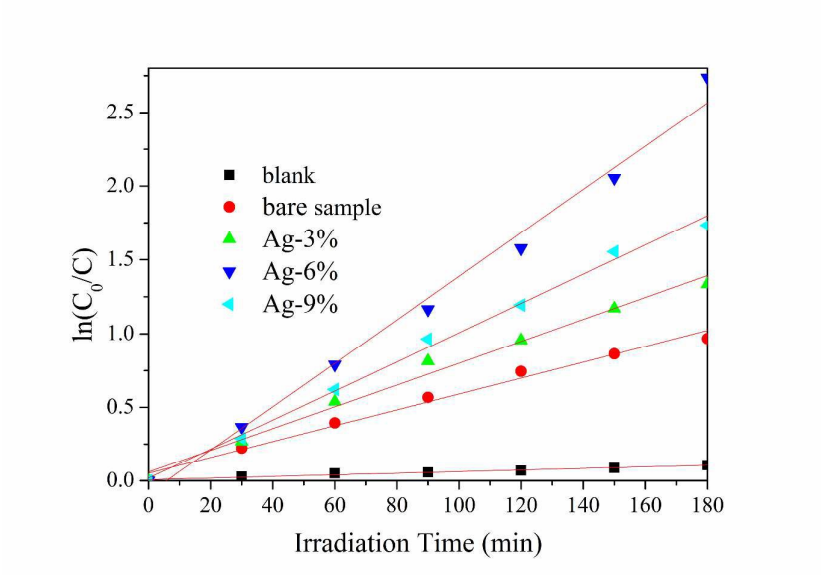

Fig. 6 linear plots of ln(C_0/C) versus time.

Table 1 Band-gap energy, photodegradation efficiency, Kinetic constants and regression coefficients of prepared samples in RhB degradation simulated sunlight irradiation

Samples	E_g (eV)	Photodegradation	Kinetic constant (min^{-1})	R^2
blank	/	9.87%	5.54E-4	0.9704
bare	2.70	61.93%	5.40E-3	0.9815
Ag-3%	2.26	73.62%	7.40E-3	0.9861
Ag-6%	2.20	93.54%	1.47E-2	0.9874
Ag-9%	2.14	82.32%	9.89E-3	0.9946

According to former study[39], RhB has visible-light screening effect. As seen in Fig 5a, RhB aqueous solution has a strong absorbance at the wavelength from 450 nm to 600 nm. When the concentration of the dye is high, a significant amount of visible light would be absorbed by the dye molecules rather than by the catalysts, and thus the efficiency of the catalytic reaction is reduced. As shown in Fig. 5b, the blank sample has much lower degradation efficiency than those with catalysts added; and it meant that in RhB degradation, the effect of self-sensitization is much less than that of photocatalysis. To get a further confirmation of no self-sensitization, four 3 W monochromatic lights (λ = 420 nm) instead of the 500 W Xe lamp were used as the light source for the photodegradation of RhB over the bare $Bi_2O_{2.33}$ and Ag-6% $Bi_2O_{2.33}$. This is due to RhB has no absorbance at the wavelength of 420 nm (Fig. 5a). As shown in Fig. 7, the RhB photodegradation efficiencies over the bare $Bi_2O_{2.33}$ and Ag-6% $Bi_2O_{2.33}$ were 68.98% and 97.36%, respectively; while no self-degradation of RhB occurred under the same condition. The results confirmed that the photocatalytic activity enhancement of the prepared catalysts is not induced by the self-sensitization effect.

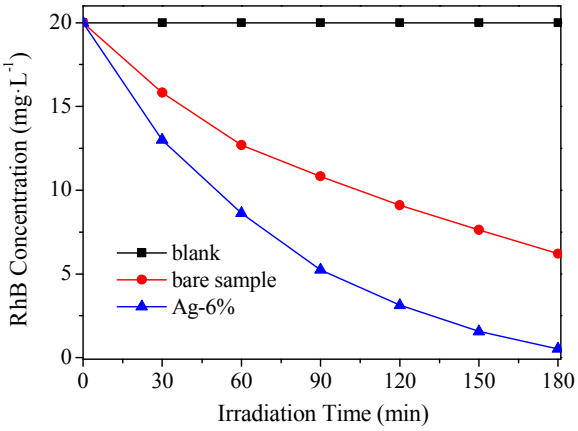

Fig. 7 Photocatalytic degradations of RhB over bare $Bi_2O_{2.33}$ and Ag-6% $Bi_2O_{2.33}$ under irradiation of monochromatic light (λ = 420 nm)

Further photocatalytic degradation experiments were carried out using Ag-6% to test the stability and reusability of the as-synthesized photocatalysts. The catalyst (Ag-6%) was reused for five times under the same conditions (Fig.8). The photodegradation efficiencies of RhB for the five cycles are 93.54%, 92.50%, 92.25%, 92.20% and 92.20%, respectively. Ag-6% demonstrates a relatively good stability in five cycles, which is of great importance for promising and practical application of such photocatalyst.

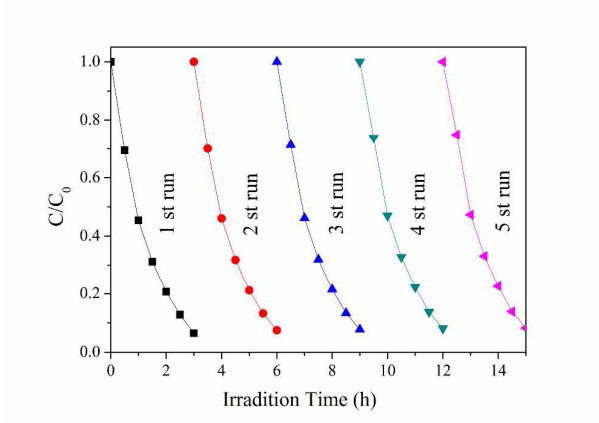

Fig. 8 The photodegradation of RhB by Ag-6% for five cycles.

Furthermore, reactive species trapping experiments were performed to investigate the reactive oxidizing species in the photocatalytic process. ·OH and $O_2^{\cdot-}$ were detected by EPR technology (with DMPO). As $O_2^{\cdot-}$ was very unstable in water and slow reaction with DMPO, the involvement of $O_2^{\cdot-}$ was examined in methanol.[40] Figure 9 shows EPR trap signals (with DMPO) of Ag-6% $Bi_2O_{2.33}$ in two different dispersions. Figure 9a shows that four characteristic peaks of DMPO-·OH in the range of 3330-3400 nm were observed in aqueous dispersions of Ag-6% $Bi_2O_{2.33}$ under simulated sunlight irradiation but no such signals were detected in dark. The intensity ratio of the four characteristic peaks is nearly 1: 2: 2: 1, and it can be inferred the existence of ·OH during the photocatalytic process.[41,42] Furthermore, Figure 9b shows that six characteristic peaks of DMPO-$O_2^{\cdot-}$ species were also detected in methanol dispersions of Ag-6% $Bi_2O_{2.33}$ under simulated sunlight irradiation but very weak nearly none signals were detected in dark. The intensity of the six characteristic peaks is nearly the same, and it can be inferred the existence of $O_2^{\cdot-}$ during the photocatalytic process.[41,42] EPR results indicated that certain light irradiation is crucial to the generation of ·OH and $O_2^{\cdot-}$ species and directly confirmed that both ·OH and $O_2^{\cdot-}$ are produced on the surface of Ag-6% $Bi_2O_{2.33}$ under simulated sunlight irradiation.

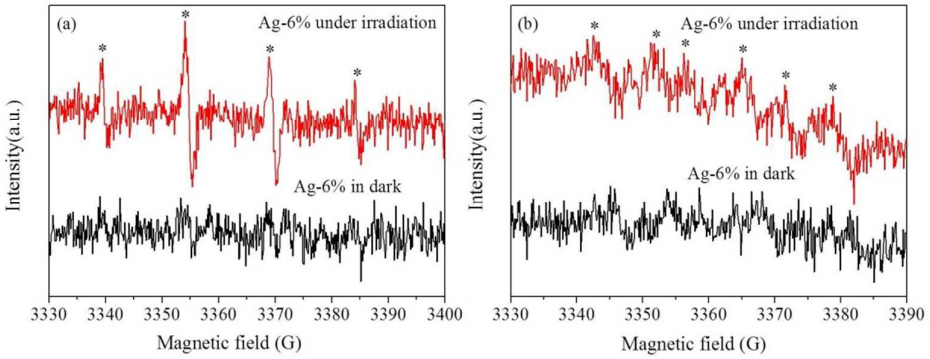

Fig. 9 EPR spectra of the reactive oxidizing species trapped by DMPO in Ag-6% $Bi_2O_{2.33}$ aqueous dispersions (a) and methanol dispersions (b)

3.5 Mechanism of photocatalytic activity

The photocatalysis principle of semiconductor is usually elucidated by photogenerated electrons and holes together. A probable mechanism of photocatalytic reaction occurring in the surface of $Bi_2O_{2.33}$ with 6% Ag content under simulated sunlight illumination is illustrated in Scheme 1. When photons with an energy ≥2.20 eV are absorbed by $Bi_2O_{2.33}$, photogenerated electrons (e^-) are aroused and transferred from valence band (VB) to conduction band (CB) across the band gap, resulting in holes and electrons in VB and CB, respectively. Electrons was then transferred to the surface of photocatalyst and react with adsorbed O_2 to generate superoxide radical anions ($O_2^{\cdot-}$), which combines with H_2O to form H_2O_2 afterwards; and H_2O_2 combines with electrons on the surface of photocatalysts to form ·OH. Holes react with OH^- or H_2O to generate hydroxyl radicals (·OH). The active oxidizing species ($O_2^{\cdot-}$ and ·OH) play significant roles in degrading adsorbed RhB molecules nearby, driving the photodegradation of RhB molecule. The RhB degradation occurs in two competitive processes: one is stepwise N-de-ethylation, and the other is the destruction of conjugated structure[43]. In the photodegradation process, these two degradation processes both took place, and the destruction of conjugated structure was the main way. After the conjugated structure of RhB was destructed, two other processes, opening-ring and mineralization followed, and some organic acidic molecules appeared in the system, which were finally mineralized to water and carbon dioxide[44].

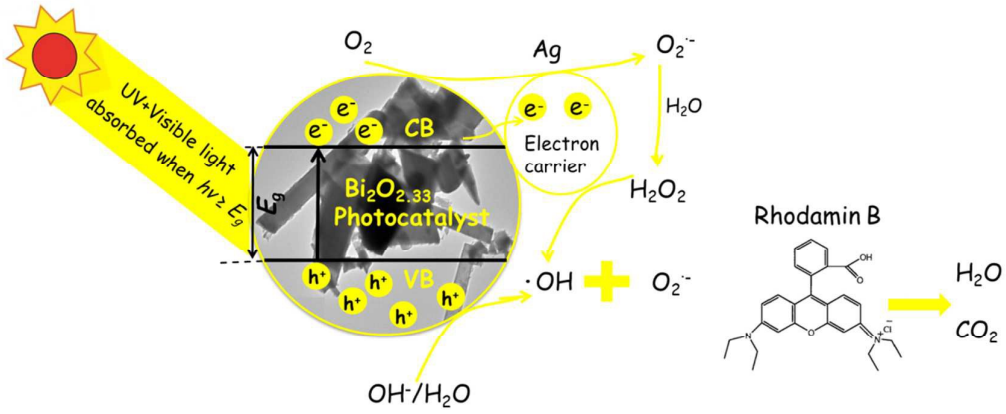

Scheme 1 Digram of light excited electron-hole separation and the photogradation process.

Accordingly, the enhanced photocatalytic activity for Ag-doped $Bi_2O_{2.33}$ could be attributed to the improved capacity of generation of electron-hole pair efficiently. Doping appropriate Ag can induce defects on the shallow surface of photocatalyst, which could become the center of electron or hole traps, or act as the center of charge carrier recombination which in turn captures the photogenerated electrons in the bulk phase[45]. However, excessive Ag in the bulk phase can also work as the recombination centers of electron-hole pairs which have negative effect on photo catalysis reaction[46]. This may be the explanation for the result that 6% Ag-doped $Bi_2O_{2.33}$

was observed to exhibit the highest activity other than 9% Ag-doped $Bi_2O_{2.33}$ in RhB degradation experiments. Moreover, the structure of Ag-doped $Bi_2O_{2.33}$ affords an attachment for RhB molecules and shortens the distance of electron transition from the inner to the surface, which ensures high flux and rapid RhB diffusion. Such structure also has positive effect on the separation of photoelectrons from holes and the degradation efficiency of RhB. On the other hand, the recombination of photogenerated electrons and holes was efficiently suppressed, improving the quantum efficiency. As a consequence, more oxidative species are generated and result in higher photocatalytic performance.

4 Conclusions

$Bi_2O_{2.33}$ and Ag-doped $Bi_2O_{2.33}$ were successfully synthesized via a facile and chemical strategy, and their optical property and photocatalytic performance were examined for the first time. It is found that Ag-doped $Bi_2O_{2.33}$ exhibit enhanced photocatalytic activity than bare $Bi_2O_{2.33}$. The Ag-6% sample yields the highest RhB removal ratio of 93.54%. Also, the modified $Bi_2O_{2.33}$ also exhibits a favorable stability and reusability; after five cycles, Ag-6% sample could still maintain a degradation yield of 92.20%. As such, the prepared Ag-doped $Bi_2O_{2.33}$ seems a promising photocatalyst with high photocatalytic activity and stability, showing a great potential in the field of environmental remediation.

Acknowledgement

This work was financially supported by the Fundamental Research Funds for Central Universities (Grant No. DUT852018).

References

[1] Y. Sun, W. Wang, L. Zhang and Z. Zhang, *Chem. Eng. J.*, 2012, **211-212**, 161-167.

[2] A. K. Chakraborty, S. B. Rawal, S. Y. Han, S. Y. Chai and W. I. Lee, *Appl. Catal. A-Gen.*, 2011,**407**, 217-223.

[3] H. Y. Jiang, G. G. Liu, M. Li, J. J. Liu, W. B. Sun, J. H. Ye and J. Lin, *Appl. Catal. B-Environ.*, 2015, **163**, 267-276.

[4] W. J. Wang, X. Q. Chen, G. Liu, Z. R. Shen, D. H. Xia, P. K. Wong and J. C. Yu, *Appl. Catal. B-Environ.*, 2015, **176-177**, 444-453.

[5] F. L. Zheng, G. R. Li, Y. N. Ou, Z. L. Wang, C. Y. Su and Y. X. Tong, *Chem. Commun.*, 2010, **46**, 5021-5023.

[6] L. Zhou, W. Z. Wang, H. L. Xu, S. M. Sun and M. Shang, *Chem.-Eur. J.*, 2009, **15**, 1776-1782.

[7] P. Marija, K. Aleksandar, B. Biljana, R. Milena, M. Branko, R.-M. Ana and R. Marko, *Mater. Lett.*, 2010, **64**, 2247-2250.

[8] S. Anandan, G.-J. Lee, P.-K. Chen, C. Fan and J. J. Wu, *Ind. Eng. Chem. Res.*, 2010, **49**, 9729-9737.

[9] H. Y. Jiang, K. Cheng and J. Lin, *Phys. Chem. Chem. Phys.*, 2012, **14**, 12114-12121.

[10] H. Y. Jiang, G. G. Liu, T. Wang, P. Li, J. Lin and J. H. Ye, *RSC Adv.*, 2015, **5**, 92963.

[11] K. Brezesinski, R. Ostermann, P. Hartmann, J. Perlich and T. Brezesinski, *Chem. Mater.*, 2010, **22**, 3079-3085.

[12] G. P. He, C. L. Xing, X. Xiao, R. P. Hu, X. X Zuo and J. M. Nan, *Appl. Catal. B-Environ.*, 2015, **170-171**, 1-9.

[13] M. M. Mohamed and A. A. Saleh, *Micropor. Mesopor. Mater.*, 2015, **204**, 62-72.

[14] S. Swati, U. Ahmad, K. M. Surinder and K. K. Sushil, *Ceram. Int.*, 2015, **41**, 3355-3364.

[15] J. M. Zhang, Z. F. Zhang, Y. Y. Zhang, C. M. Li, X. G. Sun, H. Y. Si, Z. Peng and Y. T. Li, *Mater. Express*, 2015, **5**, 336-342.

[16] M. Faisala, A. A. Ibrahima, H. Bouzid, S. A. Al-Sayari, M. S. Al-Assiri and A. A. Ismail, *J. Mol. Catal. A: Chem.*, 2014, **387**, 69-75.

[17] T. P. Gujar, V. R. Shinde, C. D. Lokhande, R. S. Mane and S. H. Han, *J. Power Sources*, 2006, **161**, 1479-1485.

[18] L. Leontiea, M. Caraman, M. Delibas and G. I. Rusua, *Mater. Res. Bull.*, 2001, **36**, 1629-1637.

[19] X. L. Gou, R. Li, G. X. Wang, Z. X. Chen and D. Wexler, *Nanotechnology*, 2009, **20**, 495-501.

[20] G. L. Fang, G. Chen, J. Q. Liu and X. Wang, *J. Phys. Chem. C*, 2010, **114**, 864-867.

[21] X. J. Huang, J. Yan, F. L. Zeng, X. L. Yuan, W. J. Zou and D. S. Yuan, *Mater. Lett.*, 2013, **90**, 90-92.

[22] H. M. Guan, X. D. Zhang and Y. Xie, *J. Phys. Chem. C*, 2014, **118**, 27170-27174.

[23] V. Frutha, M. Popab, D. Bergerc, C. M. Ionicaa and M. Jitianua, *J. Eur. Ceram. Soc.*, 2004, **24**, 1295-1299.

[24] R. Irmawati, M. N. Noorfarizan Nasriah, Y. H. Taufiq-Yap and S. B. Abdul Hamid, *Catal. Today*, 2004, **93-95**, 701-709.

[25] S. R. G. Carrazan, C. Martin, V. Rives and R. Vidal, *Spectrochim Acta A*, 1996, **52**, 1107-1118.

[26] M. Faisal, S. B. Khan, M. M. Rahman, A. Jamal and M. M. Abdullah, *Appl. Surf. Sci.*, 2012, **258**, 7515-7522.

[27] S. B. Khan, M. Faisal, M. M. Rahman and A. Jamal, *Talanta*, 2011, **85**, 943-949.

[28] H. Zhang, G. Wang, D. Chen, X. J. Lv and J. H. Li, *Chem. Mater.*, 2008, **20**, 6543-6549.

[29] J. He, I. Ichinose, T. Kunitake, and A. Nakao, *Langmuir*, 2002, **18**, 10005-10010.

[30] B. Wiley, Y.G. Sun, B. Mayers and Y.N. Xia, *Chem. Eur.*, 2005, **11**, 454–463.

[31] Y. X. Tang, P. X. Wee, Y. K. Lai, X. P. Wang, D. G. Gong, P. D. Kanhere, T. T. Lim, Z. L. Dong and Z. Chen, *J. Phys. Chem. C* , 2012, **116**, 2772–2780.

[32] M. R. Elahifard, S. Rahimnejad, S. Haghighi and M. R. Gholami, *J. Am. Chem. Soc.*, 2007, **129(31)**, 9552–9553.

[33] M. Ge, Y. Li, L. Liu, Z. Zhou and W. Chen, *J. Phys. Chem. C*, 2011, **115**, 5220-5225.

[34] N. T. Hahn, S. Hoang, J. L. Self and C. B. Mullins, *ACS Nano*, 2012, **6**, 7712-7722.

[35] S. Iyyapushpam, S. T. Nishanthi and D. P. Padiyan, *J. Alloy Compd.*, 2013, **563**, 104-107.

[36] L. Shan, G. Wang, D. Li, X. San, L. Liu, L. Dong and Z. Wu, *Dalton Trans.*, 2015, **44**, 7835-7843.

[37] Q. Huang, S. Zhang, C. Cai and B. Zhou, *Mater. Lett.*, 2011, **65**, 988-990.

[38] J. Xu, W. Meng, Y. Zhang, L. Li and C. Guo, *Appl. Catal. B-Environ.*, 2011, **107**, 355-362.

[39] H. Wang, S. Li, L. Zhang, Z. Chen, J. Hu, R. Zou, K. Xu, G. Song, H. Zhao, J. Yang and J. Liu, *RSC Adv.*, 2013, **15**, 9011.

[40] L. S. Zhang, K. H. Wong, H. Y. YIP, C. Hu, J. C. Yu, C. Y. Chan and P. K. Wong. *Environ. Sci. Technol.*, 2010, **44**, 1392−1398.

[41] W. W. Wang , T. W. Ng, W. K. Ho, J. H. Huang, S. Liang, T. C. An, G. Y. Li, J. C. Yu and P. K. Wong, *Appl. Catal. B-Environ.*, 2013, **129**, 482−490

[42] X. F. Yang, H. Cui, Y. Li, J. L. Qin, R. Zhang and H. Tang, *ACS Catalysis*, 2013, **3**, 363−369

[43] J. Li, X. Zhang, Z. Ai, F. Jia, L. Zhang and J. Lin, *J. Phys. Chem. C*, 2007, **111**, 6832-6836.

[44] Z. He, S. Yang, Y. Ju and C. Sun, *J. Environ. Sci.*, 2009, **21**, 268-272.

[45] Y. Li, S. Peng, F. Jiang, G. Lu and S. Li, *J. Serb. Chem. Soc.*, 2007, **72**, 393-402.

[46] K. Zhang, D. Jing, Q. Chen and L. Guo, *Int. J. Hydrogen Energy*, 2010, **35**, 2048-2057.

Ag doped $Bi_2O_{2.33}$ Microrods: Photocatalytic Activity Investigation

Xiaojuan Wang,[a] Alei Zhu,[a] Zhiyi Li[a] and Zhijun Liu[a*]

[a] R&D Institute of Fluid and Powder Engineering, Dalian University of Technology, Dalian 116024, China

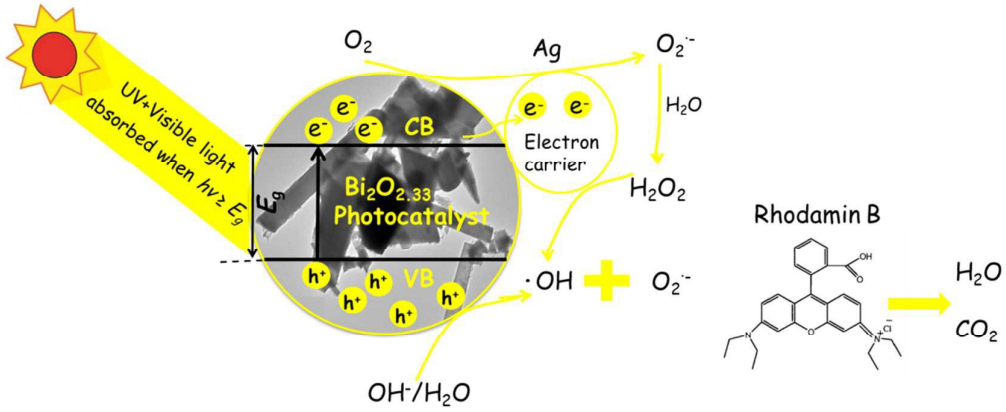

This paper presents the research of synthesized Ag doped $Bi_2O_{2.33}$ sheets by a facile method, and the investigation of the products photocatalytic ability.

* Corresponding author: E-mail: liuzj@dlut.edu.cn, Tel.&Fax: ++86-411-84986285